

## ARTICLE OPEN

## Parameterizing a borosilicate waste glass degradation model

William L. Ebert<sup>1</sup> and James L. Jerden Jr.<sup>1</sup>

Borosilicate waste glass degradation models must quantify the effects of the solution composition on the dissolution rate. Here, we present results of modified ASTM C1285 tests conducted at 90 °C with AFI and LRM glasses to determine whether dependencies of dissolution rates on the pH, Al, and Si concentrations must be included. Solution compositions were modified from those generated by glass dissolution alone by adding small amounts of  $K_4SiO_4$  glass,  $Al(OH)_3 \cdot 2H_2O$ , and a concentrated NaOH solution when the tests were initiated. Results show rate laws for the initial and resumption regimes must include pH dependences, but the residual rate can be modeled independent of the pH, Al, and Si concentrations. Triggering the resumption rate probably depends on the pH, Si, and Al concentrations and perhaps other aspects of the glass composition. A waste glass degradation model using is being parameterized using tests with a range of waste glass compositions to quantify these dependencies.

*npj Materials Degradation* (2019)3:31 | <https://doi.org/10.1038/s41529-019-0093-2>

## INTRODUCTION

The degradation rates of borosilicate glass waste forms when contacted by seepage water in breached waste packages will be used to define radionuclide source terms in contaminant transport calculations performed to assess the combined performance of the engineered and natural systems and ensure regulatory dose limits will be met throughout the service life of a disposal facility.<sup>1,2</sup> Glass degradation includes the dissolution of glass constituents into solution and the transformation of glass to secondary phases through either restructuring or coupled dissolution/precipitation processes. Various laboratory tests have shown that the degradation rates of borosilicate glasses representing likely waste form compositions are affected by both solubility and mass transfer limits. The experimentally observed degradation process is commonly described as occurring in three stages as the system evolves over time.<sup>1,3,4</sup> This is illustrated by the curves in Fig. 1a, where the abscissa represents the transformation of glass to an assemblage of thermodynamically stable secondary phases and the ordinate represents the fraction of glass degraded as the transformation progresses.<sup>3</sup> The slopes of the curves essentially represent the instantaneous glass dissolution rates attained as the system evolves and the rate-controlling process changes. The solution composition and the glass surface composition and structure all change as the glass degrades and different secondary phases are generated over time. Although the degradation process involves several coupled processes and a sequence of alteration phases may be generated, the overall behavior commonly observed in laboratory testing is well represented by this simple model. Stage 1 represents the degradation under dilute solution conditions wherein both solubility and transport effects are negligible and glass dissolution occurs at a kinetically controlled rate that depends primarily on the glass composition, temperature, and solution pH. Stage 2 represents the slowing dissolution owing to attenuation of the kinetic rate by solution feedback effects, wherein solubility limits result in the formation of a clay-like surface alteration layer that may act as a transport barrier that further slows glass dissolution.

The combined effects of solubility and transport limits can slow Stage 2 degradation to a very low rate that is commonly referred to as the residual rate. Both reaction affinity-based models<sup>5–7</sup> and mass transport-based models<sup>8,9</sup> successfully quantify Stage 2 dissolution behavior and the transition from a nearly constant Stage 1 rate to a nearly constant residual rate as degradation occurs. Stage 3 refers to the resumption of dissolution at a rate much higher than the residual rate that has been observed to occur in tests with many glasses coincidentally with the precipitation of secondary phases (usually zeolites such as analcime or phillipsite).<sup>10–12</sup> The generation of a phase that is more readily formed than those constituting the alteration layer triggers the resumption of dissolution at a higher rate. That higher rate is referred to herein as the Stage 3 rate. The growth of new phases that are thermodynamically more stable than the glass increases the reaction affinity for glass dissolution and may destabilize the surface alteration layer such that the glass degradation rate increases significantly relative to the residual rate, although it remains much slower than the Stage 1 rate. Dissolution of the glass (and perhaps also dissolution of the surface alteration layer) provides components required for the new secondary phase(s) to grow and the rates become coupled. This is how the glass transforms to stable alteration phases. Figure 1a is drawn to illustrate changes in the glass dissolution kinetics between the different reaction stages, but neither the fraction reacted nor the reaction progress are drawn to scale.

The generation of secondary phase that result in Stage 3 degradation behavior has not been observed in tests with all surrogate waste glasses or under all test conditions. The residual rate has persisted through the longest test duration in those cases.<sup>13,14</sup> The failure of appropriate secondary phases to nucleate precludes Stage 3 behavior. The conditions that trigger and maintain Stage 3 behavior (i.e., the nucleation and growth of rate-affecting secondary phases, respectively) remain to be determined and taken into account in glass degradation models. Likewise, the effect of the glass composition on the assemblage of phases that form and Stage 3 behavior remain to be quantified. It was recently

<sup>1</sup>Argonne National Laboratory, 9700 S. Cass Ave., Lemont, IL 60439, USA  
Correspondence: William L. Ebert (ebert@anl.gov) or James L. Jerden Jr. (jerdjen@anl.gov)

Received: 10 September 2018 Accepted: 25 July 2019

Published online: 29 August 2019

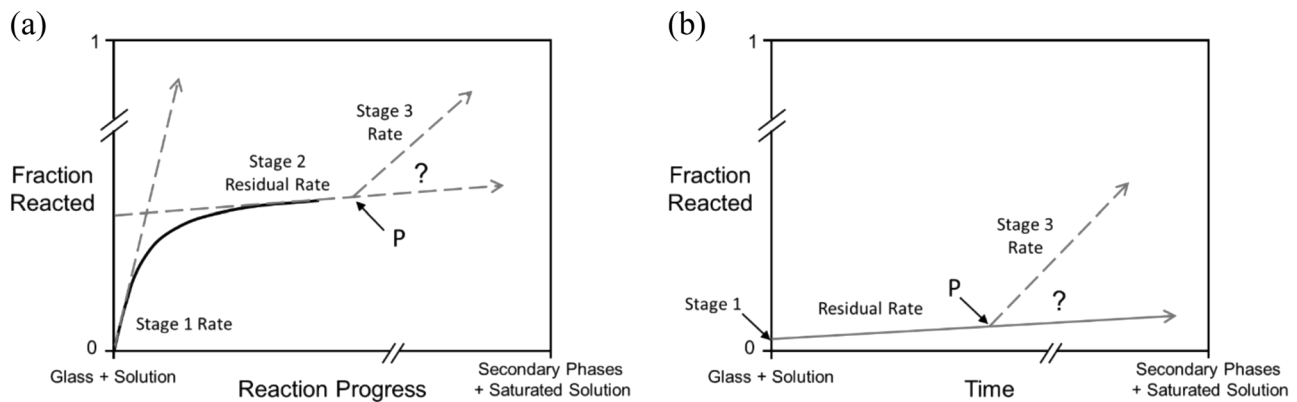


**Fig. 1** Schematic representations of glass dissolution behavior **a** to differentiate rates controlled by different mechanisms and **b** to simulate degradation of disposed waste glass

suggested that the composition and structure of the alteration layer generated during Stage 2 will affect whether zeolites triggering Stage 3 behavior will form or not.<sup>15,16</sup> Whereas most laboratory tests are conducted as closed systems, the influx of seepage water and container corrosion will affect the solution composition and provide nutrients for secondary phase formation and growth. Therefore, the full range of possible environmental conditions must be considered when predicting long-term glass degradation behavior, not only conditions generated by dissolution of the glass itself. For example, degradation of concrete barriers in the engineered disposal facility could cause the pH in seepage water to be much higher than those generated by glass dissolution during laboratory tests.

Different models have been developed to represent the degradation behavior of waste glasses in a disposal system over the long times required for radionuclide isolation. These models tend to emphasize either (1) thermodynamic control based on the reaction affinity for glass dissolution in an evolving solution chemistry or (2) kinetic control based on mass transfer through evolving surface alteration layers. Most rate equations were developed based on experimental observations of Stage 1 and Stage 2 behaviors and Stage 3 behavior has been modeled using ad hoc modifications of those equations.<sup>9,17</sup> However, experimental observations indicate the Stage 3 rate remains nearly constant (within experimental uncertainty limits) as the small amounts of glass used in most laboratory tests are completely dissolved;<sup>14,18,19</sup> neither the diffusion-based nor the reaction affinity-based models developed to represent Stage 2 are consistent with a constant Stage 3 rate. Furthermore, a constant Stage 3 rate is counter-intuitive because the surface areas of glass and secondary phase(s) change throughout the transformation.

A process model that is consistent with key observations of Stage 3 behavior was developed based on theories for incongruent mineral dissolution in which the glass dissolution and secondary phase precipitation kinetics are coupled through the transfer of common species from the glass to the secondary phase.<sup>20,21</sup> The common solution couples the dissolution and precipitation processes. A generic formulation of the rate equation in that model is

$$rate_{coupled} = \frac{rate_f^{(glass)} rate_f^{(secondary\ phase)}}{rate_f^{(glass)} + rate_f^{(secondary\ phase)}} \left[ 1 - \exp\left(\frac{\Delta G^{(glass)} + \Delta G^{(secondary\ phase)}}{RT}\right) \right], \quad (1)$$

where “secondary phase” refers to the thermodynamically most stable secondary phase in the system. This has the same general form as the reaction affinity model, wherein a kinetic rate term is attenuated by a thermodynamic affinity term (in brackets). The

terms  $\Delta G^{(glass)}$  and  $\Delta G^{(secondary\ phase)}$  represent the free energy changes for dissolving glass constituents into solution and for growing the most stable secondary phase from solution, respectively. The sum of those terms represents changes in the free energy of the system as it evolves from the initial state in Fig. 1a (glass with no secondary phases), through perhaps several intermediate states as different secondary phases form, and culminating in the final state in Fig. 1a, at which point the glass has completely transformed to stable secondary phases. The terms  $rate_f^{(glass)}$  and  $rate_f^{(secondary\ phase)}$  represent the kinetic (forward) rates for the glass dissolution and secondary phase precipitation and growth reactions. Discontinuities will occur each time a new secondary phase forms that establishes new values of  $\Delta G^{(secondary\ phase)}$  and  $rate_f^{(secondary\ phase)}$ . Glass dissolution may be coupled to the precipitation rates of several secondary phases and the relative effect of each phase may change as the transformation proceeds. However, the most-significant change in the coupled dissolution rate occurs when the first zeolite forms (indicated by Point P in Fig. 1a). The free energy differences between increasingly more-stable zeolites that may form by Ostwald ripening are small relative to the free energy difference between the glass and the first-formed zeolite. Therefore, changes in the Stage 3 rate beyond Point P are expected to be within experimental uncertainty. Interruptions in the supply of a nutrient provided by an external source would significantly affect the Stage 3 behavior.

It is likely that different secondary phases trigger and maintain Stage 3 dissolution behavior: Stage 3 is probably triggered by the nucleation of a kinetically favored phase that serves as a precursor for a different thermodynamically favored phase, the growth of which controls the Stage 3 rate. The transition from glass dissolution being coupled with two (or more) secondary phases appears to occur quickly based on experimental results, but is probably not instantaneous. The finite time span and transition can be modeled as occurring instantaneously at Point P, but the dependencies of  $rate_f^{(secondary\ phase)}$  values for the nucleating phase that triggers Stage 3 and the stable phase that maintains the Stage 3 rate on the solution composition can be different. The tests discussed herein were conducted to determine those dependencies.

We speculate that the relative surface areas of glass and secondary phases do not significantly affect the coupled glass dissolution rate during Stage 3 because changes in the individual dissolution and precipitation rates in the kinetic term (which is outside the brackets in Equation 1) compensate for the changing surface areas and maintain a constant coupled rate. The same mechanism may also control the residual rate, in which case the glass dissolution rate is coupled with the low precipitation rates of phases comprising the alteration layer, such as clays. The

difference between the residual and Stage 3 rates is that the rapid precipitation of zeolites does not attenuate the kinetic rate to the same extent as does the slow precipitation of clays.

Because it is impossible to measure the individual precipitation and dissolution rates or the surface areas of the glass or secondary phases, the kinetics that is observed experimentally as the residual and Stage 3 rates must be determined empirically from test results. The dashed lines in Fig. 1a illustrate limiting rates for the Stage 1, residual, and Stage 3 glass degradation behaviors. Both reaction affinity-based and mass transfer-based models quantify the deviation in the dissolution rate from an initial limiting maximum rate (when the reaction affinity is one or before a diffusion barrier forms) to an eventual limiting minimum rate when the reaction affinity is nearly zero or when the diffusion layer is very thick. Variance in the time required to attain the residual rate is calculated based on the evolution of the reaction affinity or mass transfer over time. We refer to the use of these limiting rates without explicitly tracking the time dependences as the Stage 3 model<sup>21</sup> and are using laboratory tests to determine limiting rates and the dependencies of the rates and when the rate changes on environmental variables. As will be shown in the following, the limiting residual and Stage 3 rates are being determined by regression fits to subsets of test data showing residual or Stage 3 dissolution behavior and when the behavior changes.

The semi-empirical approach described herein was developed to take Stage 3 degradation behavior into account within the glass degradation model used to calculate radionuclide source terms in contaminant transport models.<sup>22–24</sup> Those calculations use time-averaged property values for the environmental values and glass dissolution rate that may change for each time step. The time required to evolve from Stage 1 behavior to residual rate behavior (and the uncertainty in determining when that occurred) is negligible relative to the duration of the time steps used for performance assessments, which is typically on the order of 200–1000 years. The residual and Stage 3 rates are derived from the time dependences of test results and the y-intercept of the line fit to the residual rate represents the release during Stage 1 and until the residual rate is attained.

Although this approach is unnecessarily simplistic for modeling glass dissolution on the time scale of laboratory experiments, it is appropriate for modeling glass dissolution for times required to assess the performance of waste disposal facilities over regulated containment periods. Contaminant transport simulations that can span a million years commonly use time steps of several hundred years, for which the computational costs of representing glass dissolution kinetics in detail are not justified. Detailed representations of transitions between rate-controlling processes are not necessary and might not be implementable. The approach described herein captures the mechanistic aspects of glass corrosion needed to predict long-term glass degradation behavior and the impacts of key environmental variables to provide reliable source term values for radionuclides released as glass degrades that can be used in transport calculations.

Figure 1b shows the proposed use of the Stage 1, residual, and Stage 3 rates derived from test results as described above to model glass dissolution behavior at a more representative scale showing the fractions of glass degraded during the different reaction stages. Dissolution during Stage 1 is represented by the stoichiometric dissolution of a small mass of glass that depends on the temperature and pH of the seepage water accumulating in a breached waste package. The initial composition and temperature of the seepage water and its accumulation rate will be determined for each disposal system in a separate model based on interactions of local groundwater with engineered materials such as concrete liners and bentonite backfill. Differences in the dependencies of the amounts of glass dissolved at the Stage 1, residual, and Stage 3 rates and the Stage 3 trigger on those

variables must be quantified in the glass degradation model. In the Stage 3 model, Stage 1 dissolution occurs in 1 day after sufficient seepage water has accumulated in a breached waste package. The composition of the water within the breached package is modified by glass dissolution and tracked by the model to calculate dissolution rates used in subsequent time steps. Glass dissolution beyond 1 day is modeled to occur at the residual rate until the Stage 3 rate is triggered at Point P; both of those rates and when (and if) the Stage 3 trigger occurs depend on the solution composition.

Glass degradation during the residual and Stage 3 regimes is simulated using two steps.<sup>24</sup> In the first step, glass is dissolved into solution stoichiometrically at a rate that is a function of the temperature, pH, and composition of the seepage water. In the second step, the dissolved species are distributed between the solution and a solid phase by using element-specific partitioning coefficients. The solid phase represents the surface alteration layer during the residual rate regime and represents both the surface alteration layer and assemblage of secondary phases during the Stage 3 regime. The partitioning coefficient values used in the residual and Stage 3 regimes were determined from the differences between the glass stoichiometry and solution compositions measured in tests conducted with a range of glass compositions.<sup>22,24</sup> The seepage water that accumulates in the breached package is treated as a homogeneous well-mixed solution, the volume and composition of which are updated after each time step in the contaminant transport model. The transition from the residual rate to the Stage 3 rate at Point P in Fig. 1b is presently modeled using the mathematical form of a solubility product for the rate-affecting secondary phase (which is not identified) with threshold concentrations of solution species that are commonly observed to affect the Stage 3 trigger and rate in laboratory tests. Those tests indicate slow initial nucleation of the rate-affecting secondary phases (or their precursors) may delay the Stage 3 trigger after the threshold concentrations have been exceeded. The duration of the delay is impossible to predict and is neglected in the Stage 3 model developed for contaminant transport.

The cumulative release over the three stages of glass degradation illustrated in Fig. 1b can be expressed as the sum of releases during each stage of glass degradation:

$$\text{Cumulative Release} = \text{release1} + \sum_1^P \text{rateR} t_{T5} + \sum_P^\delta \text{rate3} t_{T5} \quad (2)$$

where *release1* is a constant representing the mass released during the time step in which sufficient seepage water first contacts the glass, and *rateR* and *rate3* represent the residual and Stage 3 rates controlling glass dissolution before and after Stage 3 is triggered. The summations are over the time steps, where  $t_{T5}$  is the duration of the time step, and  $P$  and  $\delta$  represent the time steps after Stage 3 has been triggered and when the glass has been completely transformed to secondary phases, respectively. The dependencies used in the equations for *release1*, *rateR*, *rate3*, and to determine when to trigger Stage 3 in the glass degradation model (Point P) are being determined based on the results of laboratory tests conducted for that purpose.

This paper summarizes the results of an initial series of tests conducted to develop and demonstrate the approach to parameterize the rate equations and the Stage 3 trigger used in the degradation model and determine the environmental dependencies to be included. The glasses were selected to highlight environmental effects on two aspects being assessed: LRM glass was used to provide a relatively high residual rate and AFCI glass was used to represent glasses showing Stage 3 behavior. These tests are used to determine the environmental dependencies to be included in the rate laws. Similar tests with glasses representing a range of waste glass compositions will be

**Table 1.** Matrix of imposed conditions PCTs (target values)<sup>a</sup>

Added K <sub>4</sub> SiO <sub>4</sub> , g	Added Al(OH) <sub>3</sub> ·H <sub>2</sub> O, g	Imposed initial pH(RT)	Glass and test number	
			AFCI3	LRM3
0.09	0.10	10.5, 11.5, 12.5	X <sup>b</sup> ,X,X	−1, −2, −3
	0.20	10.5, 11.5, 12.5	X,X,X	−11, −12, −13
0.14	0.05	9.5, 10.5, 11.5, 12.5	−1, −2, −3, −4	X,X,X,X
	0.10	9.5, 10.5, 11.5, 12.5	−5, −6, −7, −8	X, −4, −5, −6
	0.20	9.5, 10.5, 11.5, 12.5	−9, −10, −11, −12	X, −14, −15, −16
0.20	0.10	10.5, 11.5, 12.5	X,X,X	−7, −8, −9
	0.20	10.5, 11.5, 12.5	X,X,X	−17, −18, −19

<sup>a</sup>Test numbers corresponding to initially imposed Si, Al, and pH(RT) conditions listed as “−1, −2, etc”

<sup>b</sup>“X” indicates test not conducted under those conditions

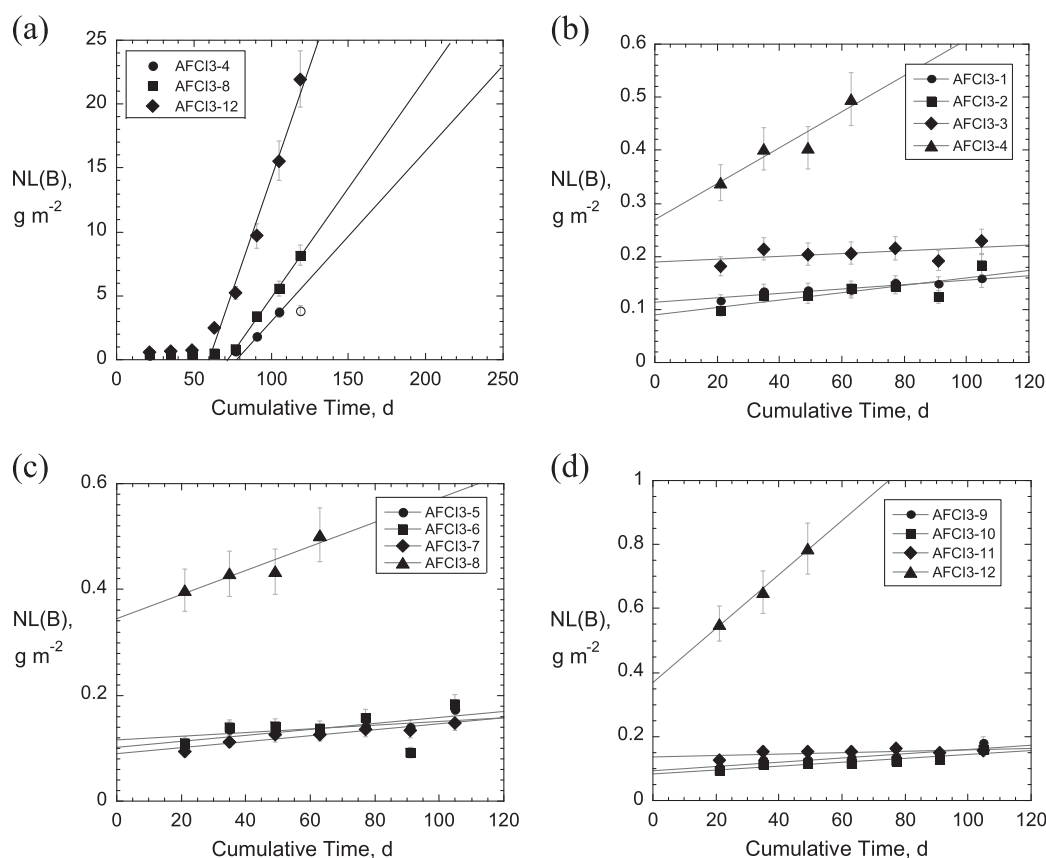


**Fig. 2** Plots of calculated NL(B) for imposed conditions PCTs with AFCI glass: **a** tests AFCI3-4, −8, and −12 with imposed initial pH 12.5, **b** tests AFCI3-1, −2, −3, and −4 with about 0.05 g Al(OH)<sub>3</sub>·2H<sub>2</sub>O, **c** tests AFCI3-5, −6, −7 with ~0.10 g Al(OH)<sub>3</sub>·2H<sub>2</sub>O, and −8, and **d** tests AFCI3-9, −10, −11, and −12 with ~0.20 g Al(OH)<sub>3</sub>·2H<sub>2</sub>O. Error bars show estimated test uncertainty

used to quantify the sensitivities of the parameter values to both the glass composition and environmental variables and recommend ranges for use in repository models.

## RESULTS AND DISCUSSION

Series of tests were conducted with LRM and AFCI glasses and different amounts of added K<sub>4</sub>SiO<sub>4</sub> glass and Al(OH)<sub>3</sub>·2H<sub>2</sub>O and different initial pH values. The conditions used in each test are summarized in Table 1 to relate the indexes used to identify tests conducted under particular imposed conditions. A 3 is included after the glass identifier to indicate tests in this study were modified to promote Stage 3 behavior and an “X” is included in

Table 1 to indicate no test was conducted under those conditions. For example, test LRM3-2 included LRM glass, 0.09 g added K<sub>4</sub>SiO<sub>4</sub> glass, and 0.10 g added Al(OH)<sub>3</sub>·2H<sub>2</sub>O, and the demineralized water leachant was adjusted to about pH 11.5 when the test was initiated. Tests results are presented using these identifiers.

The boron concentrations measured in the test solutions were used to quantify the extents of glass dissolution because they were likely not affected by additives used to vary the pH, Al, K, Na, and Si concentrations. The boron concentrations were used to calculate normalized mass losses to directly compare all test results (see Methods). The results of tests with AFCI glass are plotted as the cumulative NL(B) v the cumulative test duration in Fig. 2. Figure 2a shows the results of three tests conducted with

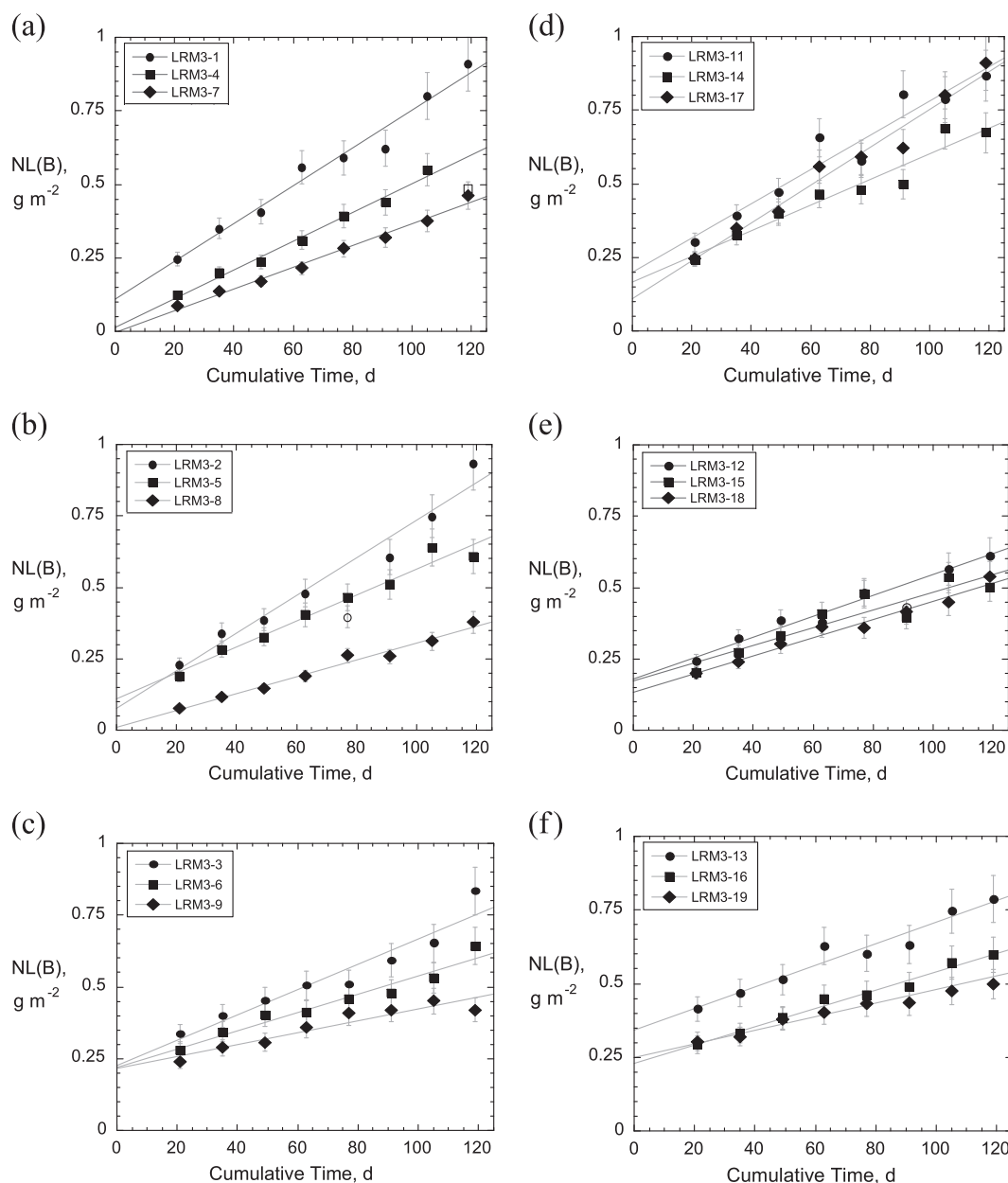


**Fig. 3** Comparison of NL(B) values for imposed conditions PCTs conducted with LRM glass, 0.10 g reagent  $\text{Al}(\text{OH})_3 \cdot 2\text{H}_2\text{O}$ , and about **a** 0.09 g  $\text{K}_4\text{SiO}_4$  glass, **b** 0.14 g  $\text{K}_4\text{SiO}_4$  glass, or **c** 0.20 g  $\text{K}_4\text{SiO}_4$  glass, and with LRM glass, 0.20 g reagent  $\text{Al}(\text{OH})_3 \cdot 2\text{H}_2\text{O}$ , and about **d** 0.09 g  $\text{K}_4\text{SiO}_4$  glass, **e** 0.14 g  $\text{K}_4\text{SiO}_4$  glass, or **f** 0.20 g  $\text{K}_4\text{SiO}_4$  glass at imposed solution pH values of pH 10.5 (circles), pH 11.5 (squares), or pH 12.5 (diamonds). Error bars show estimated test uncertainty

imposed initial pH values of 12.5 that all triggered to Stage 3 within 85 days. Test AFCI3-12, which had the greatest amount of added  $\text{Al}(\text{OH})_3 \cdot 2\text{H}_2\text{O}$ , triggered first and had the highest Stage 3 rate. Test AFCI3-4 had the least added  $\text{Al}(\text{OH})_3 \cdot 2\text{H}_2\text{O}$  of the three and the lowest Stage 3 rate. Figs 2b-d show the cumulative NL(B) values for tests conducted with similar amounts of added  $\text{Al}(\text{OH})_3 \cdot 2\text{H}_2\text{O}$  through 105 days and linear regressions. The slopes of the linear fits represent the residual rates and the y-intercepts represent the release attributed to Stage 1 dissolution in the Stage 3 model. The residual rates are similar for tests conducted at imposed pH values of 9.5 (circles), 10.5 (squares), and 11.5 (diamonds), but differ for tests conducted at imposed pH values of 12.5 (triangles) prior to Stage 3. The residual rates were attained before the first sampling at 21 days under all test conditions. For modeling purposes, it is assumed that the residual rate was attained within 1 day and that the y-intercept of the regression

line approximates the value of NL(B) after 1 day. In this way, the y-intercept represents the total amount of glass that dissolved prior to when the dissolution rate decreased to the residual rate.

Figure 3 shows the results of tests with LRM glass grouped by common pH and common amounts of added  $\text{Al}(\text{OH})_3 \cdot 2\text{H}_2\text{O}$ . None of the test results for LRM glass indicate that Stage 3 dissolution behavior occurred and the regression lines show constant residual rates through 119 days (within the 10% test uncertainty shown by the uncertainty bars). In general, the slopes and y-intercepts are slightly higher in tests conducted at higher imposed pH values, but similar in tests with different amounts of added  $\text{K}_4\text{SiO}_4$  glass and  $\text{Al}(\text{OH})_3 \cdot 2\text{H}_2\text{O}$ .

Examination of the reacted solids at the end of each test showed an abundance of secondary phases formed in the three tests with AFCI glass that degraded in Stage 3. Secondary phases were not detected in the other tests with AFCI glass that did not

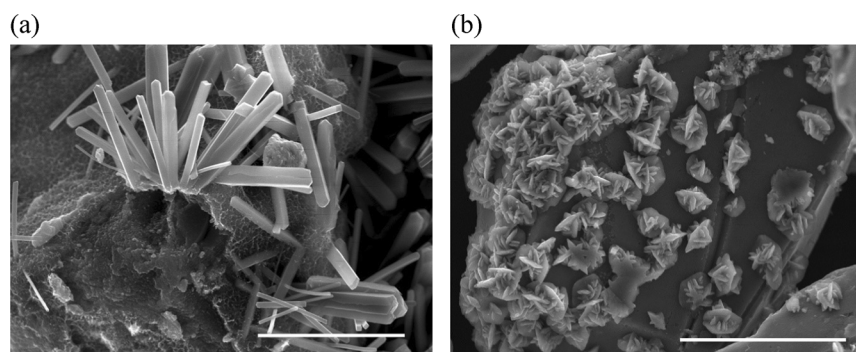


**Fig. 4** Secondary phases generated in tests. **a** AFCl3-12, scale bar = 30  $\mu\text{m}$ , and **b** LRM3-16, scale bar = 50  $\mu\text{m}$

trigger Stage 3. Crystalline secondary phases were also detected in some tests with LRM glass, even though the solution results did not indicate that Stage 3 behavior had occurred. Representative scanning electron microscopy (SEM) photomicrographs of secondary phases formed on reacted particles are shown in Fig. 4. The secondary phase formed in tests with AFCl glass was identified as phillipsite ( $\text{Na,K,Ca}_{1-2}(\text{Si,Al})_8\text{O}_{16}\cdot 6(\text{H}_2\text{O})$ ) based on morphology, composition, and X-ray diffraction (XRD) analysis and the secondary phase formed in tests with LRM glass was tentatively identified as chabazite ( $\text{Na}_2\text{K}_2\text{CaMg}[\text{Al}_2\text{Si}_4\text{O}_{12}]\cdot 6\text{H}_2\text{O}$ ). Calcite was also detected in tests with AFCl glass. This indicates the generation of secondary phases was not by itself sufficient to trigger Stage 3 glass dissolution in these tests, which may be an artifact of adding  $\text{K}_4\text{SiO}_4$  glass and  $\text{Al}(\text{OH})_3\cdot 2\text{H}_2\text{O}$ .

The solution pH values and concentrations of glass constituents generally increased slightly over time as the AFCl and LRM glasses dissolved at the residual rates. The correlations between the extent of glass dissolution in tests with LRM glass as quantified by the cumulative values of NL(B) and the measured pH, Al, and Si concentrations are plotted in Fig. 5. Tests conducted with the same amount of  $\text{Al}(\text{OH})_3\cdot 2\text{H}_2\text{O}$  are plotted in the same figures, tests conducted with the same imposed pH values are indicated by a common symbol: 10.5 (circles), 11.5 (squares), or 12.5 (diamonds), and symbols for tests with the same amount amounts of  $\text{K}_4\text{SiO}_4$  glass are indicated by common coloring: 0.09 g (solid), 0.14 g (open), or 0.20 g (shaded). The initial values of the pH, Al, and Si concentrations were not measured and the samplings after 21 days represent the combined amounts of Al and Si released by dissolution of  $\text{Al}(\text{OH})_3\cdot 2\text{H}_2\text{O}$ ,  $\text{K}_4\text{SiO}_4$ , and LRM glasses. The results show the combined effects of the imposed pH and Al and Si concentrations on the LRM glass dissolution rate based on NL(B), as the LRM glass is the only source of B in the test. Linear regression fits are shown by the curves in the semi-log plots. Most results are fit well, but the pH results for Test LRM3-19 deviate high.

Corresponding plots for tests with AFCl glass are shown in Fig. 6 grouped by tests with common additions of  $\text{Al}(\text{OH})_3\cdot 2\text{H}_2\text{O}$  for clarity. The Al and Si concentrations (and pH values, not shown) are linearly correlated with the cumulative NL(B) values during dissolution at the residual rate, but show different trends after Stage 3 behavior was triggered in Tests AFCl3-4, AFCl3-8, and AFCl3-12. The Si and Al concentrations are correlated and anti-correlated with NL(B), respectively, by logarithmic dependencies during Stage 3. Note that the Si and Al concentrations in the initial samplings of Tests AFCl3-4, AFCl3-8, and AFCl3-12 fall on or near the regression curves defined by the residual rates in other tests and probably represent the amounts released at the residual rate before Stage 3 is triggered. The Al concentrations in Tests AFCl3-8 and AFCl3-12 appear to reach lower limiting concentrations in the last three samplings (perhaps indicating the analytical quantitation limit) that are not well correlated with NL(B). These are shown as open triangles and were excluded from the regression fit. This

may indicate an Al solubility limit for the phase controlling the Al concentration, whether that phase is  $\text{Al}(\text{OH})_3$  or another phase. There is no indication that the Al concentration affects when the secondary phases form to trigger Stage 3 or the Stage 3 dissolution rate that results, but the decrease in the Al concentration seen prior to the Stage 3 trigger may indicate a necessary process that precedes it.

In order to assess the effects of the pH, Al, and Si concentrations on the residual dissolution rates, the values measured in the samples taken after 49 days were used as representative values corresponding to the residual rate that was determined for that test. Figure 7a shows the correlations between the Stage 3 rates measured in tests with AFCl glass and the pH(RT), Al, and Si concentration for those tests after 49 days. Uncertainty bars are drawn at  $\pm 10\%$  of the measured Al and Si concentrations and the derived rates to represent analytical uncertainty. The analytical uncertainty in the pH values is assumed to be  $\pm 0.02$  pH units and falls within the symbols. The Stage 3 rates are effectively independent of the low Al concentrations for modeling purposes but positively correlated with the pH and Si concentrations. The correlations may indicate an effect of the high glass dissolution rate in Stage 3 rate on the concentration or that the concentration may be a contributing cause of that high rate. The pH(RT) and Si concentrations measured prior to the Stage 3 triggers in the three tests showing Stage 3 behavior are plotted in Fig. 7b to differentiate between cause and effect. The horizontal lines show the measured Si concentrations are constant within analytical uncertainty until Stage 3 was triggered in each test. The approximate times at which Stage 3 was triggered in each test are indicated by the arrows; Si concentrations in samples taken after Stage 3 was triggered exceed the range of the plot. The high pH and Si concentrations maintained during the residual rate regime probably both contribute to Stage 3 being triggered, but the high Si concentrations attained after Stage 3 was triggered are a result of the high Stage 3 rate. The measured pH(RT) values decreased slightly prior to when Stage 3 was triggered and continued to decrease after Stage 3 was triggered in Test AFCl3-12. This indicates the high pH values promoted the Stage 3 trigger but the pH was not affected by the high Stage 3 rate.

The pH(RT) values and Si concentrations in the three tests are anti-correlated with the amounts of  $\text{Al}(\text{OH})_3\cdot 2\text{H}_2\text{O}$  that were added and the resulting Al concentrations. The solution compositions measured just prior to the Stage 3 triggers are summarized in Table 2 with the residual rates, Stage 3 trigger times (Point P), and Stage 3 rates. The trigger times were estimated from the intersections of the regression fits of the residual and Stage 3 rates. The pH(RT) of 11.9 and average Si concentration 5.8 mM measured in Test AFCl3-4 prior to the Stage 3 trigger are interpreted to represent the lower threshold value for each. The delay in the Stage 3 trigger relative to other tests that attained slightly higher pH(RT) and Si concentrations prior to the Stage 3 trigger is attributed to the effects of the pH and Si concentration

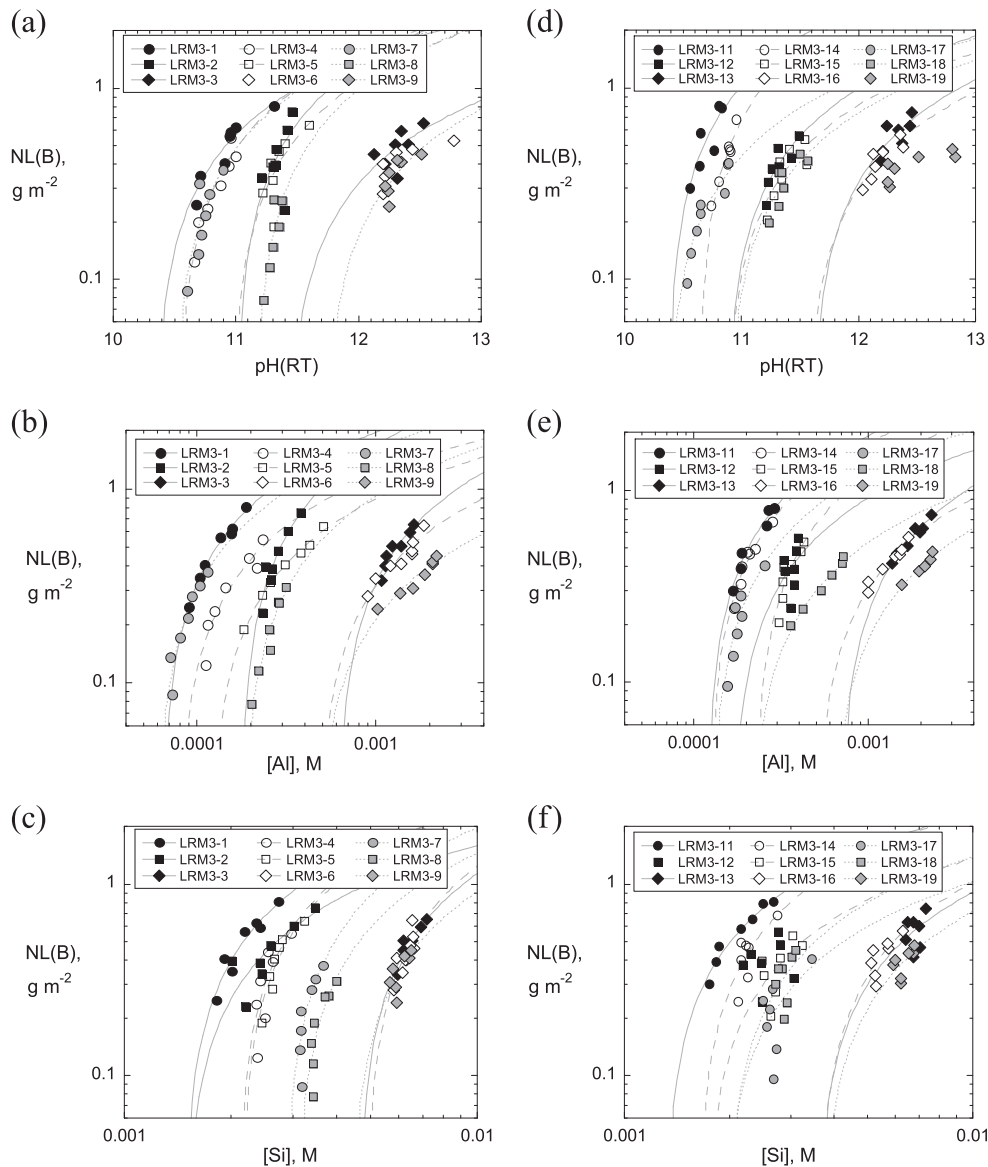


**Fig. 5** Correlations between NL(B) and Al concentrations measured in imposed conditions PCTs with LRM glass and **a–c** 0.10 g reagent Al  $(\text{OH})_3 \cdot 2\text{H}_2\text{O}$  or **d–f** 0.20 g reagent  $\text{Al}(\text{OH})_3 \cdot 2\text{H}_2\text{O}$  conducted at imposed pH values of 10.5 (circles), 11.5 (squares), or 12.5 (diamonds), and with  $\sim 0.10$  (solid symbols and solid curves), 0.14 (open symbols and dashed curves), or 0.20 g (shaded symbols and dotted curves) added  $\text{K}_4\text{SiO}_4$  glass. Curves show linear regression fits

on the nucleation kinetics of the secondary phase causing the rate resumption.

The residual rates measured in tests with APCI and LRM glass and the representative pH(RT), Al, and Si concentrations for those tests are plotted in Fig. 8. The horizontal arrows in the pH plots indicate the drift from the initially imposed pH to the measured pH values that occurred owing to glass dissolution. The NaOH solution used to impose the pH provided no buffer capacity and was overwhelmed by the effect of glass dissolution within the first test interval. The pH was likely also affected by exposure to atmospheric  $\text{CO}_2$  when the vessels were opened for sampling. Nevertheless, the initially imposed pH values provided a sufficient range of pH values to assess the effect of pH on the glass dissolution rate. The ranges of Al and Si concentrations were also less than expected, but adequate to assess their effects on the Stage 3 trigger and rate. The residual rates decreased slightly with increasing pH, Al, and Si concentrations in all test series, but the correlations are very weak (all  $R^2 < 0.5$ ) and the dependencies are near the experimental uncertainty. Because the residual rates

decrease as the glass dissolves, neglecting these weak dependences in performance calculations will provide bounding upper values for residual rates. It will also provide a conservative early bound for when Stage 3 behavior is triggered by using threshold solution concentrations and pH values.

The NL(B) values and residual rates are about 10-times higher in tests with LRM than in tests with APCI glass under similar conditions, which represents glass composition effects on the Stage 1 and residual rates. It is expected that application of this test method to a range of relevant glass compositions will result in a range of Stage 1, residual, and Stage 3 rates that can be used to determine uncertainty ranges for performance modeling. Existing databases and literature data can be used to provide insights into those ranges (e.g., ref. <sup>13</sup> and <sup>14</sup>).

In summary, modified PCTs conducted with APCI and LRM glasses at 90 °C in leachants with various imposed pH values and added Al and Si were used to assess the effects of those variables on the glass dissolution rates. The glass dissolution rates were derived from the time dependence of NL(B) values calculated

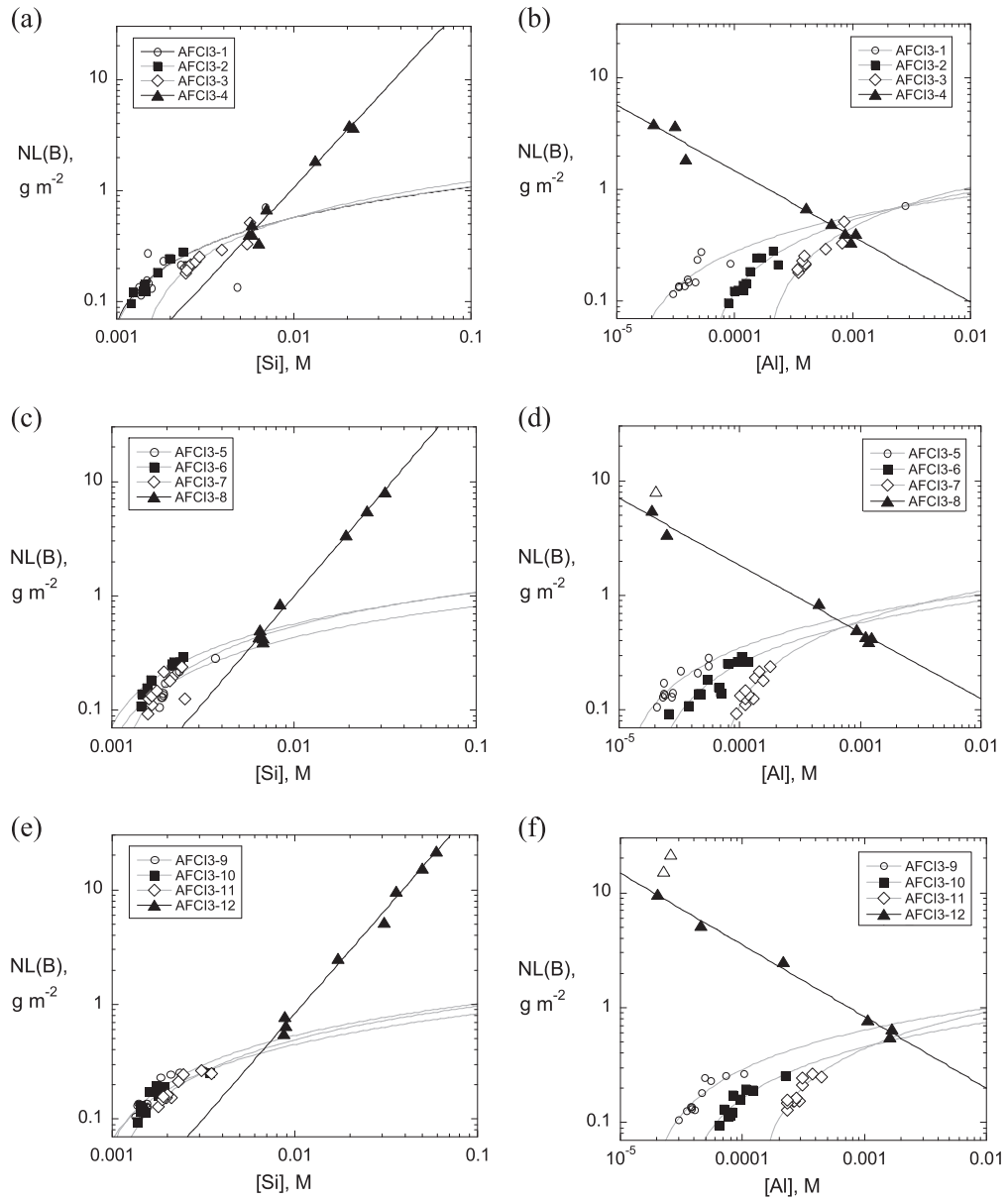


**Fig. 6** Correlations between NL(B) and pH, Al, and Si concentrations in imposed conditions PCTs: **a** Si and **b** Al concentrations in tests AFCI3-1, -2, -3, and -4, **c** Si and **d** Al concentrations in tests AFCI3-5, -6, -7, and -8, and **e** Si and **f** Al concentrations in tests AFCI3-9, -10, -11, and -12. Curves show regression fits

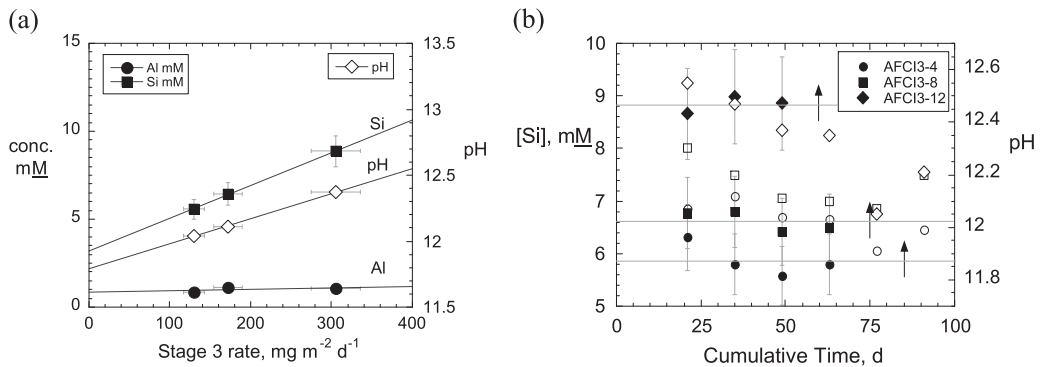


**Fig. 7** Correlations in tests with AFCI glass between **a** pH(RT), Al, and Si concentrations measured at 49 days with Stage 3 rates and **b** pH(RT) and Si concentrations measured at 49 days with cumulative test duration. Error bars show estimated test uncertainty



using concentrations measured in periodic samplings of the test solutions. The residual and Stage 3 rates were determined from the slopes of linear regressions for the series of samplings and the y-intercepts of the residual rate fits were used to determine the Stage 1 rates. The residual rates for both glasses were essentially independent of the three variables, but the Stage 1 rates (based

on the y-intercepts) and both the Stage 3 trigger and Stage 3 rates observed in three tests with AFCI glass were affected by the pH value. The results indicate the residual rate can be represented by using a constant value in performance models, but the Stage 1 and Stage 3 rate laws require pH dependency terms. The Stage 3 trigger depends on the pH and Si concentration with threshold values of about pH 11.9(RT) and 5.8 mM total Si for AFCI glass. The influence of the Al concentration remains uncertain: it decreased significantly prior to the occurrence of Stage 3 but was not correlated with the Stage 3 trigger. Stage 3 was triggered in tests with AFCI glass but not in tests with LRM glass that attained the same solution pH. This may be due to differences in the glass compositions or an artifact of the additives. The modified PCT method employed in these tests is appropriate for determining the pH and Si dependencies for other relevant glass compositions and the sensitivities to the waste glass composition. Tests with other glasses may provide insights into why Stage 3 behavior did not occur in these tests with LRM glass.

**Table 2.** Solution compositions prior to Stage 3 triggers, trigger times, and Stage 3 rates for AFCI glass

Test No.	Solution composition prior to trigger		Residual rate $\text{g m}^{-2} \text{d}^{-1}$	Stage 3 trigger, days	Stage 3 rate, $\text{g m}^{-2} \text{d}^{-1}$
	Si, mM	pH (RT)			
AFCI3-4	5.8	11.9	0.0034	85	0.13
AFCI3-8	6.6	12.1	0.0013	80	0.17
AFCI3-12	8.8	12.4	0.0084	60	0.30

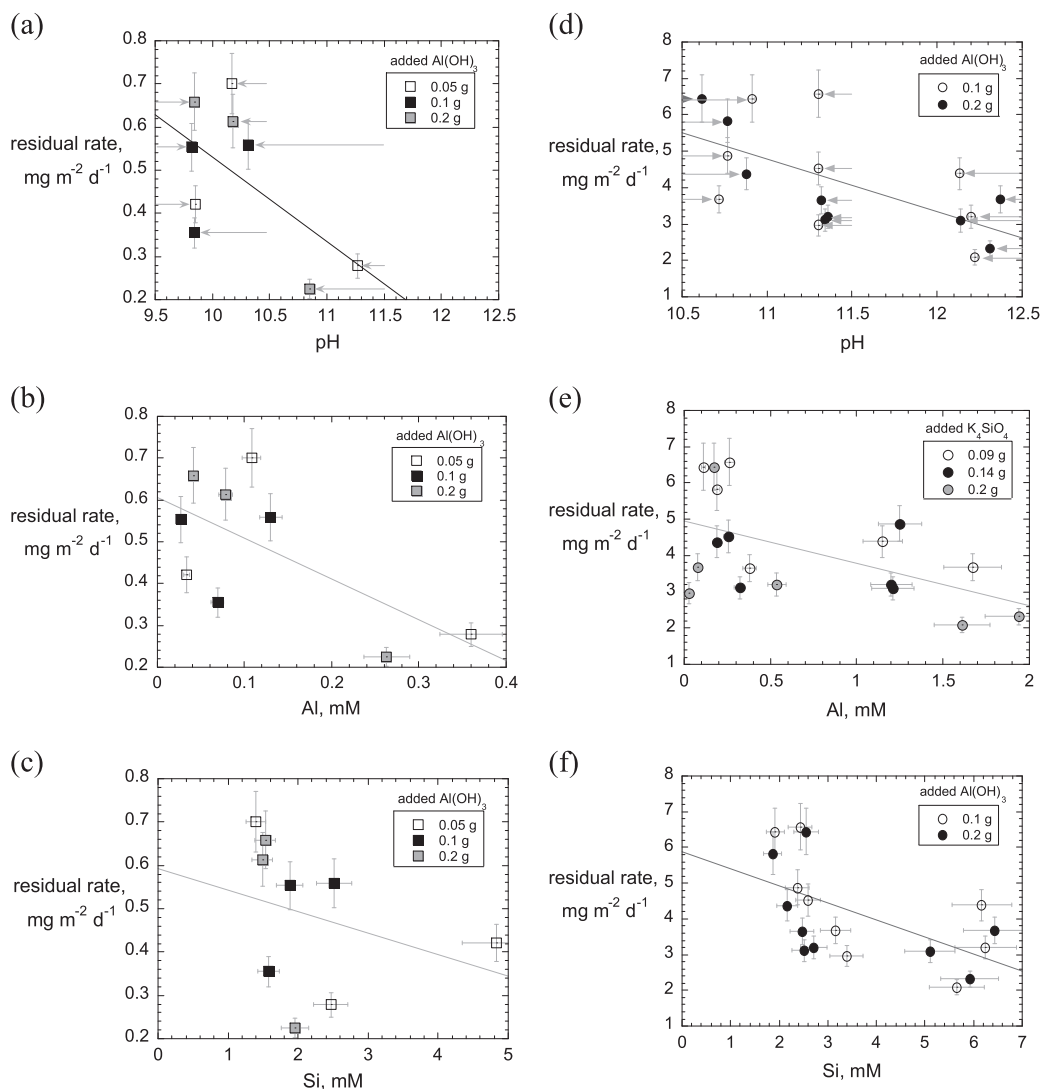


**Fig. 8** Linear correlations between residual rates for imposed conditions PCT with AFCI glass and **a** pH(RT) values, **b** Al concentrations, and **c** Si concentrations and with LRM glass and **d** pH(RT) values, **e** Al concentrations, and **f** Si concentrations measured in individual tests after 49 days

to the use of crushed glass that provides a high glass surface area-to-solution volume (S/V) ratio. Tests were conducted with LRM glass<sup>25</sup> and AFCl glass<sup>26</sup> using a modification of the PCT-B method in which small amounts of K<sub>4</sub>SiO<sub>4</sub> glass and Al(OH)<sub>3</sub>·2H<sub>2</sub>O were added with the glass being tested and demineralized water to supplement the amounts of Si and Al released during glass dissolution. The leachant pH values were then adjusted by adding small amounts of NaOH solution when the test was initiated. Different amounts of each reagent were added in each test to assess their separate effects on the dissolution behavior (see Table 1). It was expected that the added K<sub>4</sub>SiO<sub>4</sub> glass would dissolve completely but that only a small fraction of the added Al(OH)<sub>3</sub>·2H<sub>2</sub>O would dissolve to increase the Al concentration slightly. Different amounts were added to provide a sufficient range of pH and Al and Si concentrations to assess their individual effects, but not to attain specific targeted values in each test. The additional K was expected to affect the assemblage of secondary phases, but not the glass dissolution kinetics.

Dissolution rates were determined by analyzing small aliquants of the solution (~0.9 g) taken at nominally 2-week intervals (starting after 21 days) to track the evolution of the solution composition and extent of glass dissolution. The volume of solution that was removed was not replaced to avoid sudden changes in the solution composition that would have obscured the effects being assessed. This resulted in small increases in the S/V ratio during successive intervals that affected the rate slightly, but did not affect the composition dependence being measured. The effect of changing S/V ratios was taken into account by using normalized mass loss values to determine the extent of glass dissolution and dissolution rates. Solutions were diluted with demineralized water, acidified with conc. nitric acid, and analyzed by using inductively coupled plasma-mass spectrometry.

All tests were conducted with crushed (–200 + 325 mesh size fraction) glass in 100-mL Teflon vessels with demineralized water. Teflon vessels were used to facilitate frequent sampling. Using a size fraction of glass that was smaller than that commonly used in PCTs allowed for the use of larger solution volumes to reduce the impact of taking solution samples on the S/V ratios and solution compositions: tests were conducted with about 4.5 g glass in 90 mL of solution. The small amount of water lost to evaporation in the tests at 90 °C was tracked by weighing the assembled vessels weekly and replaced with demineralized water every week the solution was not sampled for analysis. Evaporative losses were < ~0.06% per week.

The normalized elemental mass losses were calculated from the concentrations measured in each sampling as

$$NL(B) = \frac{[B]}{f(B)S/V} \quad (3)$$

where  $NL(B)$  is the normalized elemental mass loss based on the measured B concentration,  $[B]$ ,  $f(B)$  is the mass fraction of B in the glass,  $S$  is the initial geometric surface area of glass in the test, and  $V$  is the solution volume. The glass surface area was based on the mass of glass added during test initiation and the calculated geometric specific surface area of the crushed glass, and the elemental mass fractions were based on the nominal glass compositions, which have been given elsewhere;<sup>25,26</sup> the mass fractions of B in AFCl and LRM glasses are 0.030 and 0.024, respectively. The effective specific surface area of each size fraction was calculated by modeling the particles as spheres with diameters equal to the average of the mesh openings for the size fraction. The initial solution volume was used in all NL (i) calculations to take the mass of material removed with the analyzed aliquants into account in the calculated cumulative amount released at each sampling. Solutions were analyzed by using inductively coupled plasma-mass spectrometry (PerkinElmer NexION 2000 or PerkinElmer Sciex ELAN DRC II).

Reacted solids recovered from some tests were examined by using SEM (Hitachi S-3000N) with energy dispersive X-ray emission spectroscopy (EDS, Thermo Scientific UltraDry) and by powder XRD (Siemens D5000).

## DATA AVAILABILITY

The data sets generated during and/or analyzed during the current study are available from the corresponding author on reasonable request.

## ACKNOWLEDGEMENTS

Solution analysis by Ms Yifen Tsai (ANL) is gratefully acknowledged. This work was funded by the US DOE Office of Nuclear Energy Nuclear Technology Research and

Development under direction of the Material Recovery and Waste Form Development campaign, Dr. Terry Todd, National Technical Director and Ms Kimberly Gray, Federal Manager. Work at Argonne National Laboratory is supported by the U.S. Department of Energy under contact DE-AC02-06CH11357.

## AUTHOR CONTRIBUTIONS

The testing approach was conceived and data analyses were performed by W.L.E. Tests and SEM analyses were conducted by J.L.J.

## ADDITIONAL INFORMATION

**Competing interests:** The authors declare no competing interests.

**Publisher's note:** Springer Nature remains neutral with regard to jurisdictional claims in published maps and institutional affiliations.

## REFERENCES

- Poinsot, C. & Gin, S. Long-term behavior science: the cornerstone approach for reliably assessing the long-term performance of nuclear waste. *J. Nucl. Mater.* **420**, 182–192 (2012).
- Rechard, R. P. & Stockman, C. T. Waste degradation and mobilization in performance assessments for the Yucca Mountain disposal system for spent nuclear fuel and high-level radioactive waste. *Reliab. Eng. Syst. Saf.* **112**, 165–188 (2013).
- Cunnane, J. C. (ed.) High-level waste borosilicate glass: a compendium of corrosion characteristics, United States Department of Energy Office of Waste Management report DOE-EM-0177 (1994).
- Vienna, J. D., Ryan, J. V., Gin, S. & Inagaki, Y. Current Understanding and remaining challenges in modeling long-term degradation of borosilicate nuclear waste glasses. *Int. J. Appl. Glass Sci.* **4**, 283–294 (2013).
- Grambow, B., and Strachan, D. M. A comparison of the performance of nuclear waste glasses by modeling. Pacific Northwest Laboratory report PNL-6698 (1988).
- Grambow, B. & Müller, R. First-order dissolution rate law and the role of surface layers in glass performance assessment. *J. Nucl. Mater.* **298**, 112–124 (2001).
- Oelkers, E. General kinetic description of multioxide silicate mineral and glass dissolution. *Geochim. Cosmochim. Acta.* **65**, 3709–3719 (2001).
- Frugier, P. et al. SON68 nuclear glass dissolution kinetics: Current state of knowledge and basis of the new GRAAL model. *J. Nucl. Mater.* **380**, 8–21 (2008).
- Minet, Y., Bonin, B., Gin, S. & Frugier, P. Analytic implementation of the GRAAL model: application to a R7T7-type glass package in a geological disposal environment. *J. Nucl. Mater.* **404**, 178–202 (2010).
- Ebert, W. L. & Bates, J. K. A Comparison of glass reaction at high and low surface area to volume. *Nucl. Technol.* **104**, 372–384 (1993).
- Fournier, M., Gin, M., Frugier, S., P & Mercado-Depierre, S. Effect of zeolite formation on borosilicate glass dissolution kinetics. *Procedia Earth Planet. Sci.* **7**, 264–267 (2013).
- Fournier, M., Gin, S. & Frugier, P. Resumption of nuclear glass alteration: state of the art. *J. Nucl. Mater.* **448**, 348–363 (2014).
- Ribet, S., Muller, I. S., Pegg, I. L., Gin, S., and Frugier, P. Compositional effects on the long-term durability of nuclear waste glasses: a statistical approach. Scientific Basis for Nuclear Waste Management XXVIII, 309 (2004).
- Jantzen, C. M. Letter Report on SRNL Modeling Accelerated Leach Testing of Glass (ALTGLASS). FCRD-SWF-2013-000339, Rev. 0., Savannah River National Laboratory, Saiken, SC (2013).
- Jantzen, C. M., Trivelpiece, C., Crawford, C., Pareizs, J. & Pickett, J. Accelerated leach testing of glass (ALTGLASS): I. Informatics approach to high level waste glass gel formation and aging. *Int. J. Appl. Glass Sci.* **8**, 69–83 (2017).
- Jantzen, C. M., Trivelpiece, C., Crawford, C., Pareizs, J. & Pickett, J. Accelerated leach testing of glass (ALTGLASS): II. Mineralization of hydrogels by leachate strong bases. *Int. J. Appl. Glass Sci.* **8**, 84–96 (2017).
- Strachan, D. M. & Neeway, J. J. Effects of alteration product precipitation on glass dissolution. *Appl. Geochem.* **45**, 144–157 (2014).
- Ebert, W. L. and Tam, S.-W. Dissolution rates of DWPF glasses from long-term PCT. Scientific Basis for Nuclear Waste Management XX, W.J. Gray and I.R. Triay (eds) pp 149–156 (1997).
- Fournier, M., Gin, S., Frugier, P. & Mercado-Depierre, S. Contribution of zeolite-seeded experiments to the understanding of resumption of glass alteration. *npj Mater. Degrad.* **1**, 17 (2017).
- Ebert, W. L. Stage 3 Model for coupled glass dissolution and secondary phase precipitation reactions. DOE NE report FCRD-MRWF-2015-000763. Argonne National Laboratory (2015).
- Ebert, W. L. Glass degradation in performance assessment models. *Mater. Res. Soc. Symp. Proc.* **1744**, 163–172 (2015).

22. Ebert, W. L. An evaluation of the ALTGLASS database for insights into modeling Stage 3 behavior. DOE NE report FCRD-SWF-2014-000616. Argonne National Laboratory (2014).
23. Ebert, W. L. Implementing the glass degradation model in generic disposal system analysis. DOE NE report FCRD-MRWFD-2015-000546. Argonne National Laboratory (2015).
24. Ebert, W. L., and Jerden, J.L. Jr. Implementation of the ANL Stage 3 glass dissolution model. DOE NE report FCRD-MRWFD-2016-000296. Argonne National Laboratory (2016).
25. Ebert, W. L. & Wolf, S. F. An interlaboratory study of a standard glass for acceptance testing of low-activity waste glass. *J. Nucl. Mater.* **282**, 112–124 (2000).
26. Neeway, J. J., Rieke, P. C., Parruzot, B. P., Ryan, J. V. & Asmussen, R. M. The dissolution behavior of borosilicate glasses in far-from equilibrium conditions. *Geochim. Cosmochim. Acta.* **226**, 132–148 (2018).



**Open Access** This article is licensed under a Creative Commons Attribution 4.0 International License, which permits use, sharing, adaptation, distribution and reproduction in any medium or format, as long as you give appropriate credit to the original author(s) and the source, provide a link to the Creative Commons license, and indicate if changes were made. The images or other third party material in this article are included in the article's Creative Commons license, unless indicated otherwise in a credit line to the material. If material is not included in the article's Creative Commons license and your intended use is not permitted by statutory regulation or exceeds the permitted use, you will need to obtain permission directly from the copyright holder. To view a copy of this license, visit <http://creativecommons.org/licenses/by/4.0/>.

© The Author(s) 2019